Morphology and Properties of Thermoplastic Polyurethane Composites Incorporating Hydrophobic Layered Silicates

Bradley Finnigan, Darren Martin, Peter Halley, Rowan Truss, Kayleen Campbell

Divisions of Chemical and Materials Engineering, University of Queensland, Brisbane, Queensland 4072, Australia

Received 3 August 2003; accepted 16 November 2004
DOI 10.1002/app.21718
Published online in Wiley InterScience (www.interscience.wiley.com).

ABSTRACT: Polyurethane (PU) composites incorporating Cloisite 15A (15A) were prepared via melt compounding and solvent casting. The melt-compounded composites had better dispersion and a smaller silicate stack size as a result of the higher shear forces associated with twin-screw extrusion. The PU microphase separation and hard domain order were greater in the melt-processed materials. At the concentrations of 15A employed in this study (≤7 wt %), the filler did not have an observable effect on the microphase texture of either the solvent- or melt-processed PU. The tensile properties of the melt-compounded materials were lower than those of their solvent-cast counterparts because of thermal degradation. The solvent-cast composite containing a 3 wt % loading of 15A displayed improved tensile strength and elongation, primarily because of plasticization by the silicate organic treatment. The addition of layered silicates with high aspect ratios increased the hysteresis and permanent set of this PU elastomer. © 2005 Wiley Periodicals, Inc. J Appl Polym Sci 97: 300–309, 2005

Key words: nanocomposites; polyurethanes; processing; SAXS; structure-property relations

INTRODUCTION

Thermoplastic polyurethanes (TPUs) are linear block copolymers consisting of alternating hard and soft segments. The hard segment is composed of alternating diisocyanate and chain-extender molecules (i.e., diol or diamine), whereas the soft segment is formed from a linear, long-chain diol. Phase separation occurs in TPUs because of the thermodynamic incompatibility of the hard and soft segments. The segments aggregate into microdomains, and this results in a structure consisting of glassy or semicrystalline hard domains and rubbery, soft domains that are below and above their glass-transition temperatures (T_g's) at room temperature, respectively. The hard domains act as physical crosslinks and impart elastomeric properties to the soft phase. Because of the absence of chemical crosslinking, TPUs are able to be processed via melt and solution methods.

Polymeric nanocomposites incorporating nanosized layered silicates have attracted a great deal of interest in recent years. Improvements in the mechanical, thermal, and barrier properties have been reported at very low filler concentrations (~1–5 wt %).[1–5] Although the mechanisms behind these improvements are not fully understood at present, it is evident that the altered properties of these materials are related to changes in polymer molecular dynamics[6,7] and crystallinity,[8] in addition to traditional filler reinforcement. An improved understanding of these mechanisms is desired to enable the design of materials with customized property profiles.

TPU nanocomposites represent a fascinating system for study because of the already complex microphase structure of TPUs. Recent investigations have shown that layered silicates can have a significant impact on the microphase structure of block copolymers.[9,10] Studies of polyurethane (PU) nanocomposites to date have largely overlooked the effect of the layered silicates on the underlying microdomain texture.[11–16] Previously, we investigated the effect of a layered silicate with a hydrophilic surface modification on the morphology and properties of two TPU host polymers varying in the hard-segment/soft-segment composition ratio.[17] In this study, TPU composites were prepared via twin-screw extrusion and solvent casting through the incorporation of Cloisite 15A (15A), a commercially available layered silicate with a relatively hydrophobic surface modification. The effect of this layered silicate on the microphase morphology and properties of the TPU was investigated in an effort to enhance the understanding of this class of materials.

EXPERIMENTAL

Materials

The PU employed in this study consisted of a 1000 g/mol poly(tetramethylene oxide) (PTMO) soft seg-

Correspondence to: D. Martin (darrenm@cheque.uq.edu.au).
Contract grant sponsor: University of Queensland (through a Postgraduate Research Scholarship).

© 2005 Wiley Periodicals, Inc.

ment and a 4,4′-methylene diphenyl diisocyanate (MDI) and 1,4-butanediol (BDO) hard segment. The hard-segment concentration was 35 wt %, and this resulted in a soft elastomer with a Shore hardness of 80A. PU was supplied by Urethane Compounds (Melbourne, Australia).

The Cloisite series of organosilicates (Southern Clay Products, Gonzales, TX) is based on a natural montmorillonite with a cation-exchange capacity of 0.92 mequiv/g. 15A has a 1.25 mequiv/g dimethyl ditallow ammonium modification, and the tallow composition is approximately 65% C_{18}, 30% C_{16}, and 5% C_{14}. 15A was dried in a vacuum oven at 80°C for 12 h before use.

Preparation

Melt compounding

PU and 15A were compounded in a Haake mini twin-screw extruder (Rheology Solutions, Melbourne, Australia) at a screw speed of 40 rpm and at a barrel temperature of 210°C. The extrudate was then compression-molded at 210°C for 3 min and cooled to room temperature for 3 min more.

Solvent casting

A 5 wt % solution of dried 15A in toluene was ultrasonicated for 2 min before being added to a 5 wt % solution of PU in dimethylacetamide (DMAc). The combined solution was then mixed vigorously for 1 min in a high-shear homogenizer, and this was followed by stirring for 1 h at room temperature with a magnetic stirrer. The mixture was then ultrasonicated for 2 min, and the films were immediately cast onto glass plates. The films were dried under a nitrogen atmosphere at 50°C for 36 h and subsequently dried *in vacuo* at 50°C for 12 h.

The solvent-cast and melt-compounded films, with thicknesses of approximately 0.5 and 1 mm, respectively, were then annealed *in vacuo* at 80°C for 12 h and left for 1 month before characterization. Composites with 15A loadings of 3 and 7 wt % were prepared.

Characterization

The molecular weights of the PUs were determined by gel permeation chromatography on a Waters Alliance 2690 separations module (Milford, MA). High performance liquid chromatography grade DMAc containing 0.03 wt % LiCl was used as the eluent, and two Styragel columns (3 HT and 6E HT, with effective molecular weight ranges of 500–30,000 and 5000 to 1 $\times 10^7$, respectively) were used for separation. Polystyrene standards were used for calibration (Pressure Chemical Co., Pittsburgh, PA).

TABLE I
Effect of Processing on Host PU Molecular Weight

	PU	
	M_n	PDI
As received	216,000	1.8
Solvent-cast	121,000	1.7
Melt-compounded	66,000	2.0

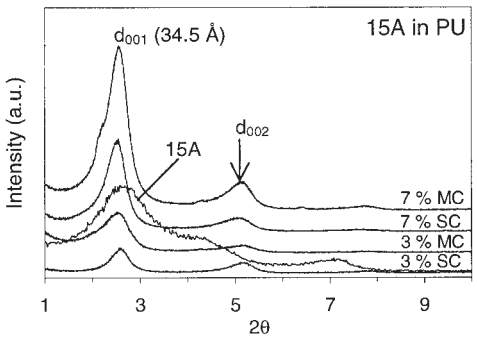

Figure 1 WAXD intensity profiles (MC = melt-compounded, SC = solvent-cast).

Differential scanning calorimetry (DSC) measurements were performed on a TA Instruments 2920 MDSC instrument. The sample weight was approximately 10 mg, and the heating rate was 10°C/min from −100 to 300°C.

Dynamic mechanical measurements were made with a Rheometric Scientific DMTA IV dynamic thermal mechanical analyzer (New Castle, DE) equipped with a tensile head and reducing force option. The analysis was performed at a frequency of 2 Hz and a heating rate of 2°C/min from −100 to 110°C.

Wide-angle X-ray diffraction (WAXD) analysis was carried out on a Bruker D8 Advance X-ray diffractometer (Karlsruhe, Germany) with Cu Kα radiation generated at 40 kV and 30 mA. The samples were scanned at 2.4°/min in the range of $2\theta = 1–40°$ with a step size of 0.02°. The 15A powder was lightly pressed and flattened to obtain a smooth surface before testing.

Small-angle X-ray scattering (SAXS) measurements were performed on a camera at the Australian National University with Cu Kα with $\lambda = 1.54$ Å. The specifications of this instrument have been described elsewhere.[18] The scattering intensity was corrected for the detector sensitivity, electronic background, sample transmission, and sample thickness.

Transmission electron microscopy (TEM) samples were cut on a Leica Ultracut S ultramicrotome (Wetzlar, Germany) with a glass knife at −100°C and were collected on 400-mesh copper grids. Images were obtained with a JEOL JEM 1010 TEM instrument (Peabody, MA) operated at 100 keV.

Tensile and hysteresis tests were carried out at 25°C on an Instron model 4505 universal testing machine (Canton, MA) with five replicates of each material.

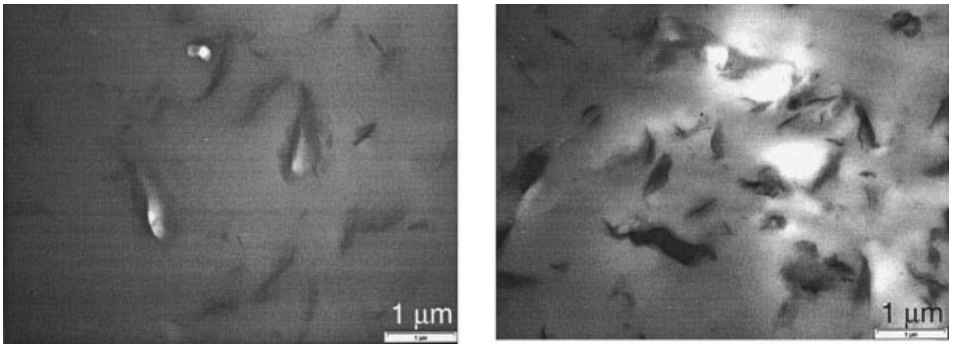

Figure 2 TEM images of solvent-cast nanocomposites: (left) 3 wt % 15A and (right) 7 wt % 15A.

Dumbbells were punched from an ATSM D 638-M-3 die. A crosshead speed of 5 mm/min was employed, and pneumatic grips were used to prevent slippage. Young's modulus was calculated from the slope at 0% strain on the tensile curve. The reported hysteresis values were measured on the fifth loading–unloading cycle. The permanent set was taken as the strain at which the zero load was measured on the unloading cycle.

RESULTS AND DISCUSSION

PU molecular weight

The number-average molecular weights (M_n's) and polydispersity indices (PDIs) of the host polymer before and after processing via solvent casting and melt compounding are given in Table I. The molecular weights of the composites were not determined to eliminate the possibly of layered silicates entering the separation columns. A significant decrease in M_n occurred during both solvent casting and melt compounding. The ultrasonic probe was identified as the cause of this decrease in the solvent-cast materials, whereas thermal and thermooxidative degradation processes associated with the melt processing of this class of PUs were responsible for the molecular weight reduction in the melt-compounded materials.[19,20] Furthermore, small extruders have been reported to impose a harsher environment on polymers than their larger counterparts because the ratio of the surface area to the volume increases with decreasing extruder size.[21] In addition to the effects of the small extruder used in this study, the PU did not contain any stabilizing additives.

X-ray diffraction

WAXD patterns of the composites and the pure organosilicate are shown in Figure 1. All the composites exhibited a well-defined diffraction peak (d_{001}) at $2\theta = 2.6°$, corresponding to the regular interlayer spacing of the organosilicate platelets. The second (d_{002}) reflection of this structure was also visible. An increase in the interlayer spacing is usually indicative of an intercalated structure (alternating polymer and silicate layers).[2] In this case, the small increase in the interlayer spacing from approximately 32.5 (15A) to 34.5 Å (composite) suggests that very little, if any, polymer intercalated the interlayer spacing. 15A is produced with an excess of a quaternary ammonium surfactant, which is not ion-exchanged to the silicate surface. Vaia et al.[22] postulated that the majority of the excess 15A surfactant is removed from the interlayer in a toluene solution. It is conceivable that the excess surfactant

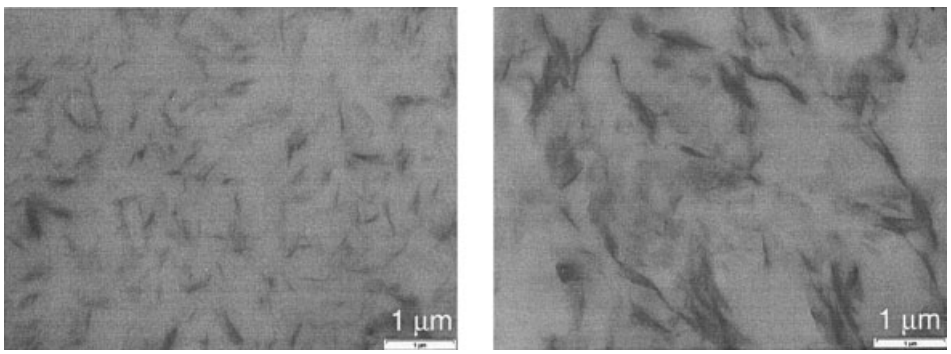

Figure 3 TEM images of melt-compounded nanocomposites: (left) 3 wt % 15A and (right) 7 wt % 15A.

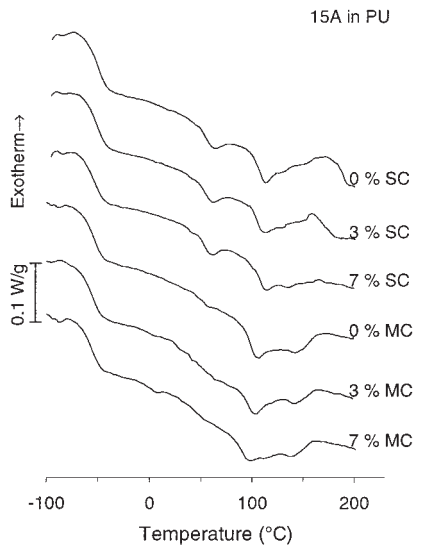

Figure 4 DSC thermograms (MC = melt-compounded, SC = solvent-cast).

was replaced by PU. Regardless of whether PU entered the interlayer or not, the small change in the interlayer spacing illustrates the low driving force for intercalation between relatively hydrophobic 15A and more hydrophilic PU.

TEM

TEM images of the composites prepared via solvent and melt processing are displayed in Figures 2 and 3, respectively. These images reveal a structure consisting of stacks of organosilicates, rather single intercalated platelets. Although the processing route did not affect the interlayer spacing measured by WAXD, it is evident from the TEM images that the stacks were smaller and more evenly distributed in the composites prepared by melt compounding. The smaller stack sizes in the melt-compounded composites were also detected qualitatively by the slightly broader full width at half-maximum values obtained from the WAXD d_{001} diffraction peaks.[22] The smaller stack size achieved by melt compounding was a result of the higher shear stresses associated with this processing technique, which promoted the fracturing of layered silicate stacks.[23] The voids that can observed in the images of the solvent-cast samples are not associated with this processing method. The voids resulted from prolonged exposure to the electron beam.

DSC

DSC thermograms are shown in Figure 4, and a summary of the DSC features is given in Table II. Strong soft-segment glass transitions at approximately −55 and −52°C were evident for the melt-compounded and solvent-cast materials, respectively. The higher T_g values of the solvent-cast materials and the smaller heat capacity step (ΔC_p) associated with the transition indicated that there were more hard segments present in the soft phase, and this hindered molecular motion. The addition of 15A did not have an observable affect on T_g, ΔC_p, or the temperature range over which the transition occurred. Dynamic mechanical thermal analysis (DMTA) provides a more sensitive measure of this transition, and these results are discussed later.

There have been numerous studies of the multiple endothermic behavior of segmented PUs.[24–29] The size and position of the melting endotherms have been linked to various factors, including the segment length,[25,30,31] hard-segment/soft-segment ratio,[30,32] and thermal history.[25,33,34] The endotherms identified in this study are labeled T1 and T2, in agreement with the nomenclature used in our previous study.[17]

A T1 endotherm was observable at approximately 68°C in the materials prepared by solvent casting. Endotherms occurring in the vicinity of this temperature have been attributed to various phenomena, including enthalpy relaxation,[28] the disordering of single MDI hard segments,[25,31] and the disordering of nonideally packed N—H···O═C hard segments in the interfacial region between the soft and hard

TABLE II
Summary of Heating Curves

			Endotherm peaks				Exotherm	
15A content	$T_{g(\text{soft})}$ (°C)	ΔC_p (J/g/°C)	T1 (°C)	T2 (°C)		Hard-phase ΔH (J/g)[a,b]	Peak (°C)	ΔH (J/g)[b]
0% SC	−52	0.40	68	113	130	21.3 ± 3.6	177.5	5.3 ± 0.9
3% SC	−52	0.40	68	110	130	19.9 ± 1.6	158	4.9 ± 1.0
7% SC	−52	0.40	68	113	136	22.8 ± 3.7	—	—
0% MC	−55	0.44	—	107	144	27.5 ± 5.5	—	—
3% MC	−55	0.44	—	101	143	36.6 ± 3.7	—	—
7% MC	−55	0.44	—	99	141	30.6 ± 6.0	—	—

[a] Enthalpy of fusion values were the sum of the T1 and T2 melting enthalpies.
[b] Enthalpies were calculated per gram of hard segment (not per gram of sample).
SC = solvent-cast; MC = melt-compounded.

phases.[35] The absence of this endotherm in the melt-compounded materials provided evidence for increased phase separation via this processing route.

A bimodal T2 endotherm occurring in the temperature range of 100–150°C was observed for all samples. The first of the endotherms (100–110°C), the so-called annealing endotherm, occurred approximately 20–30°C above the annealing temperature.[25–27] To confirm this assignment, we further annealed the samples at 110°C, and this resulted in the merging of the two endotherms at approximately 130–140°C (endotherms not shown). Although there is still some speculation surrounding the origin of this endotherm, a relatively recent study proposed that this endotherm is due to an enthalpy relaxation of the amorphous hard segment.[36] The second of the endotherms could be attributed to the disordering of the hard segments. The sum of the enthalpies associated with the T1 and T2 endotherms was larger for the melt-compounded materials, and this is further evidence for more organized hard domains. The addition of 15A did not affect the enthalpy associated with the endotherms.

A broad exotherm was observed immediately after the T2 endotherms in the host polymer and the composite containing 3 wt % 15A and prepared by solvent casting. The temperature associated with this transition decreased at a 3 wt % loading of 15A, and the exotherm vanished completely at the 7 wt % loading. Interestingly, the energy associated with this transition did not change at the intermediate 3 wt % loading of 15A. At present, the origin of this behavior is unclear. There were no subsequent melting endotherms as would be expected if this were a crystallization process. Instead, this exotherm may be related to conformational changes taking place in the hard phase after the melting endotherms. Heated SAXS/small-angle neutron scattering studies are being considered to help identify the nature of this exotherm.

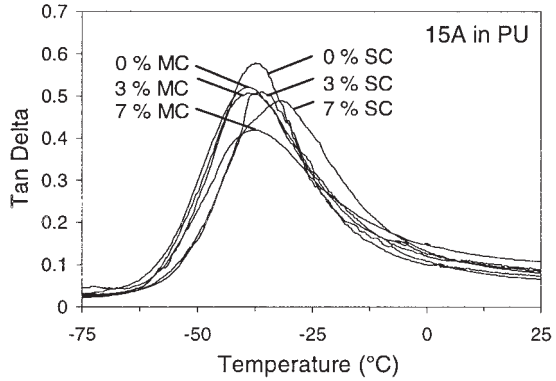

(a)

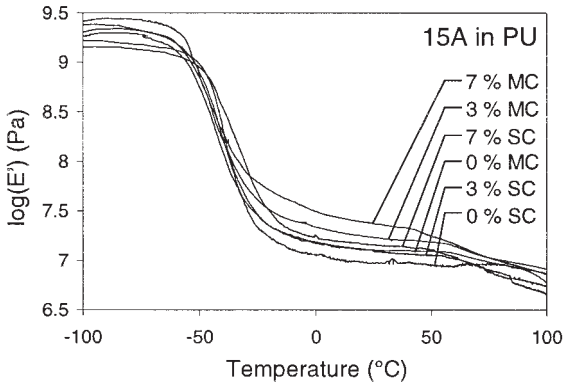

(b)

Figure 5 Dynamic mechanical data as a function of temperature: (a) tan δ and (b) E' (MC = melt-compounded, SC = solvent-cast).

TABLE III
$T_{g(soft)}$ Values Determined from DMTA

15A content (wt %)	$T_{g(soft)}$ MC	$T_{g(soft)}$ SC
0	−39	−37
3	−39	−36
7	−38	−32

MC = melt-compounded; SC = solvent-cast.

Dynamic mechanical properties

The dissipation factor (tan δ) and storage modulus (E') curves determined by DMTA are presented in Figure 5. Tan δ is equal to E''/E', where E'' is the loss modulus. The tan δ peak is associated with the soft-segment glass-transition temperature ($T_{g(soft)}$), and the peak positions are given in Table III. T_g measured via DMTA shifted to higher temperatures with respect to that measured by DSC because of its dependence on the frequency. In agreement with the DSC results, $T_{g(soft)}$ of the host polymer occurred at a higher temperature when it was prepared by solvent casting. This indicates that there were more hard segments present in the soft phase, and they hindered molecular motion. The presence of hard segments in the soft phase led to an increase in $T_{g(soft)}$ in much the same way that the crystalline portion of semicrystalline polymers increases T_g of the amorphous fraction.[37] The hard-segment T_g is often difficult to detect in this type of PU,[38] and it was not clearly observed for any of the materials studied here. In this case, the transition was probably gradual because of the broad distribution in the hard-segment lengths resulting from the one-step bulk polymerization.[39]

The addition of 15A did not alter $T_{g(soft)}$ of the composites, with the exception of the 7 wt % 15A solvent-cast sample, which displayed an increase in T_g. Organosilicates similar to 15A have been observed to impart competing effects on polymer relaxation behavior.[40,41] The layered silicates act to restrict mo-

lecular motion, whereas the alkylammonium surfactant plasticizes the polymer. Any increases in T_g that could be expected from the addition of the filler may have been offset by the plasticizing effect of the 15A surfactant. It should also be considered that fillers can loosen the molecular packing of the polymer chains and shift T_g to lower temperatures.[42]

E' of the host PU at room temperature was higher when it was prepared by melt compounding. This was probably because the hard microdomains were more cohesive, and this enhanced their fillerlike reinforcement and physical crosslinking capability. E' increased slightly with the 15A concentration. Increases in the modulus resulted from the mismatch in the elastic constants of the polymer and filler.[43] Improvements in stiffness were slightly larger for the melt-compounded composites, presumably because of the better silicate dispersion and larger effective aspect ratio of the organosilicate stacks.[44] The decrease in the height of the tan δ peak with increasing filler content was a result of the increase in E' rather than a decrease in E'' (E'' curves not shown).

SAXS

SAXS patterns of the host polymers and composites are given in Figure 6. The scattering peak at $q \approx 0.18$ $Å^{-1}$ corresponded to the interlayer spacing of the organosilicate platelets and was approximately 0.5–1 $Å^{-1}$ larger than that measured by WAXD. In addition

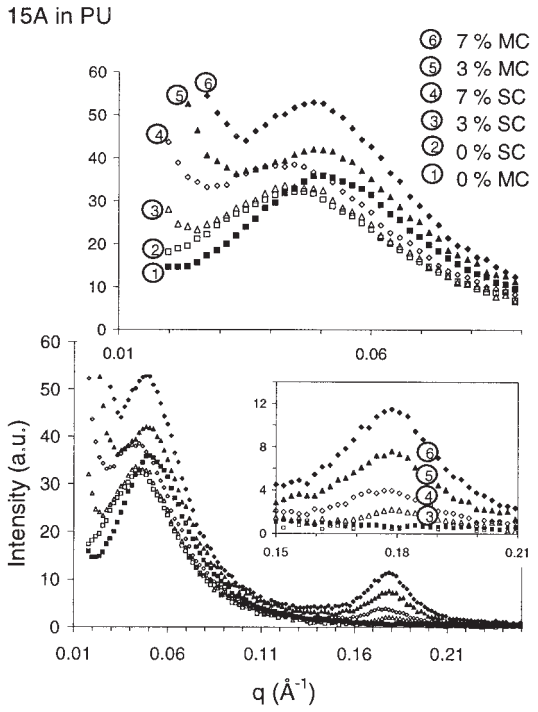

Figure 6 SAXS patterns (MC = melt-compounded, SC = solvent-cast).

TABLE IV
Interdomain Spacings

15A content	Interdomain spacing (nm)	
	$I(q)$ versus q	q^2 I(q) versus q
0% SC	13.7	10.5
3% SC	14.4	10.5
7% SC	15.2	10.5
0% MC	12.3	10.0
3% MC	13.0	10.0
7% MC	13.3	10.0

SC = solvent-cast; MC = melt-compounded; I = scattering intensity; q = scattering vector.

to the concentration of the scatterers, the orientation of the platelets has a large effect on the scattering intensity observed for a given scattering geometry.[22] The 3 wt % 15A melt-compounded composite scattered more strongly than the 7 wt % solvent-cast composite in transmission. This result suggests that melt processing and solvent processing give rise to different orientational stack distributions.[22]

The peak at $q \approx 0.05$ $Å^{-1}$ corresponded to scattering from the periodicity in the PU microdomain structure. The simplest way of estimating the periodicity or interdomain spacing (d) is through the application of Bragg's equation ($d = 2\pi/q_{max}$, where q_{max} is the maximum in the scattering curve). The d-spacings obtained from the $I(q)$–q curves and Lorentz-corrected [$q^2I(q)$ vs q] curves are given in Table IV. The reasoning for measuring the d-spacings from two styles of plots will be discussed shortly. First, the solvent-cast materials had slightly larger d-spacings than their melt-compounded counterparts. The d values obtained from the $I(q)$–q data suggests that there was also a slight increase in d with increasing 15A content, whereas the Lorentz-corrected data showed no change in the periodicity upon filler addition. The apparent increase in the d-spacing upon the addition of 15A from the $I(q)$–q plot is believed to be a result of the contribution from the lamellar silicate scattering, which showed a power-law dependence ($I \sim q^m$, $m < -2$) in this region.[22] The Lorentz correction is recommended for lamellar scattering, and so it seems reasonable to assume that the microphase periodicity was unaffected by the filler at these concentrations.

The intensity of the PU peak is related to the degree of microphase separation. Referring back to Figure 6, we can see that the melt-compounded samples were slightly more phase-separated than those prepared by solvent casting. This agreed with the DSC and DMTA results, which showed the solvent-cast materials to have slightly less hard domain order and higher $T_{g(soft)}$ values. Phase separation occurred as a result of the incompatibility between the hard and soft segments. It is believed that the solvent-cast materials were not as well phase-separated as the melt-com-

TABLE V
Summary of Tensile Properties

15A content (wt %)	Solvent-cast			Melt-compounded		
	Young's modulus (MPa)	Tensile strength (MPa)	Fail strain (%)	Young's modulus (MPa)	Tensile strength (MPa)	Fail strain (%)
0	7.5 ± 0.2	45 ± 4	1136 ± 48	7.2 ± 0.6	21 ± 4	1445 ± 97
3	9.3 ± 0.3	53 ± 2	1328 ± 8	9.2 ± 0.6	12 ± 1	964 ± 102
7	9.3 ± 0.6	34 ± 3	1299 ± 34	9.5 ± 0.8	8 ± 2	933 ± 106

pounded materials because of the DMAc solvent used during casting. The solubility parameter of DMAc was between those of PTMO and MDI/BDO, as shown in Table V.[45,46] This may have caused the hard and soft segments to be more compatible in solution and resulted in a slightly lower degree of phase separation after solvent evaporation. Phase separation may also be enhanced through hard-segment crystallization.[47] At the low casting temperature employed in this study, 60°C, the hard segment was unable to crystallize. However, this is not believed to be the cause of the reduced phase separation because the WAXD patterns (not shown) of both the melt- and solvent-processed materials exhibited an amorphous halo and no distinct crystalline peaks.[33,47] The addition of 15A resulted in an increase in the PU peak intensity and the appearance of a low-angle tail. As a first approximation, it would appear that if the silicate scattering was subtracted, the intensity of the PU peak would be roughly the same. However, a quantitative evaluation of the scattering arising from organosilicates in polymer composites "is a formidable task."[22]

Mechanical properties

Tensile curves of the host polymer and composites are presented in Figure 7, and a summary of the tensile properties is provided in Table V. In contrast to the E' results obtained via DMTA, the Young's modulus results did not display a dependence on the processing route, despite its effect on the microphase morphology, molecular weight, and, in the case of the composites, silicate dispersion. Improvements in the modulus upon silicate addition were reasonably small. The modulus was observed to increase by approximately 25% at a 3 wt % loading of 15A, and further increases in stiffness at a 7 wt % loading were small, if they occurred at all. Although an increase in the filler content was expected to increase the stiffness, such gains were probably offset by the plasticizing effect of the short-chain surfactant.[40,41]

The ultimate tensile strengths of the solvent-cast materials were significantly higher than those of their melt-compounded counterparts. The solvent-cast materials were able to undergo higher levels of chain stretching and soft-segment crystallization, as evidenced by the increased upturn in the stress–strain curves. This was primarily a result of the differences in the molecular weights resulting from the two processing routes. Considering the host polymer initially, we show in Table I that M_n of the solvent-cast PU was twice that of the corresponding melt-compounded sample. This halving of the molecular weight resulted in the melt-compounded PU having a tensile strength of 21 MPa, which was 24 MPa lower than that of the solvent-cast PU (45 MPa).

The melt-compounded composites showed a reduction in the ultimate tensile properties with increasing filler content. The reduction in the ultimate tensile properties of the melt-compounded composites could be primarily attributed to a further reduction in the PU molecular weight brought about by the degradation of the 15A alkyl quaternary ammonium surfactant. The temperature required to melt-process PU was higher than the onset of the 15A surfactant degradation temperature (~200°C). Some of the degradation products from alkyl quaternary ammonium salts, such as alkenes,[48] react readily with isocyanates, which are present in melt processing because of the normal urethane dissociation and recombination reactions that occur above 170°C.[20,25] These reactions are believed to reduce the molecular weight and lead to

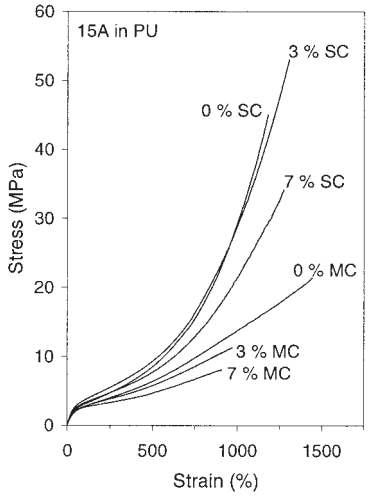

Figure 7 Stress–strain behavior (MC = melt-compounded, SC = solvent-cast).

TABLE VI
Summary of Materials Under Cyclic Conditions

	Solvent-cast				Melt-compounded			
15A (wt %)	H_{100} (%)[a]	PS_{100} (%)[b]	H_{200} (%)[a]	PS_{200} (%)[b]	H_{100} (%)[a]	PS_{100} (%)[b]	H_{200} (%)[a]	PS_{200} (%)[b]
0	9 ± 1	13 ± 1	14 ± 1	32 ± 2	11 ± 1	13 ± 1	14 ± 1	35 ± 6
3	11 ± 1	17 ± 1	16 ± 1	41 ± 1	16 ± 1	18 ± 2	19 ± 1	54 ± 7
7	14 ± 1	19 ± 1	19 ± 2	45 ± 5	21 ± 1	24 ± 2	23 ± 1	72 ± 9

[a] Hysteresis (H) was calculated on the fifth loading–unloading cycle to 100 and 200% strain.
[b] Permanent set (PS) was taken as the strain at which zero load was measured on the fifth unloading cycle to 100 and 200% strain.

reduced strength and elongation. Although some water is also released from the montmorillonite interlayer above 200°C,[48] it is believed to cause significantly less damage to the PU molecular weight than the quaternary ammonium surfactant. A PU composite incorporating 3 wt % Cloisite Na^+ (no surfactant) was prepared in our laboratories and displayed the same tensile strength as the neat PU.

The solvent-cast composite containing 3 wt % 15A exhibited improved tensile strength and elongation at break. It is believed that these improvements were a result of the 15A surfactant plasticizing PU. The plasticizing effect promoted the relaxation of local stresses, allowing the material to achieve a higher elongation at break.[49] At a 7 wt % loading, the tensile strength was reduced. The 7 wt % solvent-cast material exhibited a higher T_g values than the other samples, and this means that the mobility of the polymer chains was reduced. At higher elongations, the reduced mobility may have affected the ability of PU to undergo hard-segment fibrillation and soft-segment crystallization, and this led to a reduction in the ultimate tensile strength.[50,51] The SAXS patterns did not provide any evidence suggesting that the static microphase morphology of this sample had been altered by 15A, and this also would be expected to affect the tensile properties in some way. It is also probable that the larger organosilicate stacks (present at the 7 wt % loading) acted as flaws and led to reduced tensile strength.

Hysteresis was calculated on the fifth cycle to observe the behavior of the nanocomposites under cyclic conditions. The hysteresis and permanent set results are presented in Table VI. The hysteresis and permanent set in PU elastomers result predominantly from the plastic deformation of the hard domains.[52] The addition of layered silicates led to an increase in the hysteresis and permanent set in the materials studied here. The strain-induced stress softening of filled elastomers is known as the Mullins effect. In elastomeric, layered silicate composites, the stress softening is large because the high-aspect-ratio particles are effective at hindering the ability of the polymer chains to relax and return to their original positions.[53] The detachment of polymer chains from the filler and chain slippage over the filler surface with strain are also expected to contribute to the increased stress softening.[54–56] The higher hysteresis and permanent set of the melt-compounded composites were partly a result of their better dispersion and smaller silicate stacks that had higher effective surface areas and aspect ratios. The reduced molecular weight of the melt-compounded composites may also have contributed to the increased hysteresis and permanent set.

CONCLUSIONS

PU composites incorporating 15A were prepared via melt compounding and solvent casting. WAXD patterns revealed a small increase in the interlayer spacing, which suggested that minimal polymer intercalated the interlayer spacing. TEM images revealed the presence of stacks of organosilicates, rather than individual layers. The melt-compounded composites had better organosilicate dispersion and a smaller stack size as a result of the higher shear forces associated with twin-screw extrusion.

DSC, DMTA, and SAXS provided evidence for slightly higher phase separation and hard domain order in the melt-processed materials. The solvent-processing route produced a morphology consisting of hard microdomains that were more disordered and were centered further apart than those achieved via melt processing. At the concentrations of 15A employed in this study, the filler did not have an observable effect on the PU microphase morphology. This is not surprising because little polymer was confined in the interlayer spacing.

Although melt compounding offered better silicate dispersion than solvent casting, solvent casting must be the preferred processing route for these materials because of the elimination of PU and surfactant degradation. Improvements in stiffness were low upon silicate addition because of the modest silicate dispersion and plasticizing effect of the surfactant. The tensile properties of the melt-compounded materials were lower than those of their solvent-cast counter-

parts because of thermal degradation. In the solvent-cast composites, the tensile strength and elongation were improved at a 3 wt % loading of 15A, but the tensile strength decreased at a 7 wt % loading. The addition of layered silicates with high aspect ratios increased the stress-softening effect of this PU elastomer under cyclic straining.

In a previous study,[17] layered silicates with a hydrophilic surface modification were incorporated into the same PU. In comparison with the hydrophobic modification used here, the hydrophilic surface resulted in much higher PU intercalation and silicate dispersion and delamination on the nanoscale. This was because of the favorable enthalpic interaction between the PU and the hydroxyl functionality of the surfactant.[57–59] These studies have shown that the need for optimized processing conditions becomes less important as the strength of the interaction between the polymer and filler surface increases.

The much larger polymer–filler interface and amount of mechanically restrained polymer present in the hydrophilic nanocomposites resulted in significantly higher stiffness, hysteresis, and permanent set. The hydrophilic silicates did not have a significant impact on the PU microphase morphology, as was the case for the materials studied here. Although the ultimate tensile properties of the solvent-cast PU were improved at a 3 wt % loading of hydrophobic silicates, the hydrophilic silicates caused a decrease in the properties at this concentration. It has since been observed that the tensile properties can be improved with less than 1 wt % hydrophilic silicates. This suggests that the polymer–filler interface was too great at the 3% loading, and this led to excessively restrained polymer and reduced tensile properties. Further work investigating the influence of the hydrophilic silicate aspect ratio is expected to broaden our understanding of the mechanisms at play in these complex multiphase systems.

The authors thank Kevin Jack, Jeremy Ruggles, and John White for their helpful discussions regarding the small-angle X-ray scattering results, Michael Murphy for his assistance with the dynamic mechanical thermal analysis, and Ronda Plummer for the gel permeation chromatography results.

References

1. Kojima, Y.; Usuki, A.; Kawasumi, M.; Okada, A.; Fukushima, Y.; Kurauchi, T.; Kamigaito, O. J. Mater Res 1993, 8, 1185.
2. Alexandre, M.; Dubois, P. Mater Sci Eng 2000, 28, 1.
3. Giannelis, E. P. Adv Mater 1996, 8, 29.
4. LeBaron, P. C.; Wang, Z.; Pinnavaia, T. J Appl Clay Sci 1999, 15, 11.
5. Schmidt, D.; Shah, D.; Giannelis, E. P. Curr Opin Solid State Mater Sci 2002, 6, 205.
6. Lu, H. B.; Nutt, S. Macromolecules 2003, 36, 4010.
7. Kuppa, V.; Manias, E. J Chem Phys 2003, 118, 3421.
8. Liu, X. H.; Wu, Q. J. Eur Polym J 2002, 38, 1383.
9. Yurekli, K.; Karim, A.; Amis, E. J.; Krishnamoorti, R. Macromolecules 2003, 36, 7256.
10. Silva, A. S.; Mitchell, C. A.; Tse, M. F.; Wang, H. C.; Krishnamoorti, R. J Chem Phys 2001, 115, 7166.
11. Tortora, M.; Gorrasi, G.; Vittoria, V.; Galli, G.; Ritrovati, S.; Chiellini, E. Polymer 2002, 43, 6147.
12. Tien, Y. I.; Wei, K. H. Macromolecules 2001, 34, 9045.
13. Wang, Z.; Pinnavaia, T. J Chem Mater 1998, 10, 3769.
14. Xu, R. J.; Manias, E.; Snyder, A. J.; Runt, J. J Biomed Mater Res A 2003, 64, 114.
15. Chang, J. H.; An, Y. U. J Polym Sci Part B: Polym Phys 2002, 40, 670.
16. Chen, T. K.; Tien, Y. I.; Wei, K. H. Polymer 2000, 41, 1345.
17. Finnigan, B.; Martin, D. J.; Halley, P.; Truss, R. W.; Campbell, K. Polymer 2004, 37, 2149.
18. Aldissi, M.; Henderson, S. J.; White, J. W.; Zemb, T. Mater Sci Forum 1988, 27, 437.
19. Shieh, Y. T.; Chen, H. T.; Liu, K. H.; Twu, Y. K. J Polym Sci Part A: Polym Chem 1999, 37, 4126.
20. Yang, W. P.; Macosko, C. W.; Wellinghoff, S. T. Polymer 1986, 27, 1235.
21. Whiteside, B. R.; Martyn, M. T.; Coates, P. D.; Greenway, G.; Allen, P.; Hornsby, P. Presented at the Polymer Processing Society Annual Meeting, Melbourne, Australia, 2003.
22. Vaia, R. A.; Liu, W. D.; Koerner, H. J Polym Sci Part B: Polym Phys 2003, 41, 3214.
23. Dennis, H. R.; Hunter, D. L.; Chang, D.; Kim, S.; White, J. L.; Cho, J. W.; Paul, D. R. Polymer 2001, 42, 9513.
24. Saiani, A.; Daunch, W. A.; Verbeke, H.; Leenslag, J. W.; Higgins, J. S. Macromolecules 2001, 34, 9059.
25. Martin, D. J.; Meijs, G. F.; Gunatillake, P. A.; McCarthy, S. J.; Renwick, G. M. J Appl Polym Sci 1997, 64, 803.
26. Koberstein, J. T.; Russell, T. P. Macromolecules 1986, 19, 714.
27. Seymour, R. W.; Cooper, S. L. Macromolecules 1973, 6, 48.
28. Laity, P. R.; Taylor, J. E.; Wong, S. S.; Khunkamchoo, P.; Norris, K.; Cable, M.; Chohan, V.; Andrews, G. T.; Johnson, A. F.; Cameron, R. E. J Macromol Sci Phys 2004, 43, 95.
29. Ryan, A. J.; Macosko, C. W.; Bras, W. Macromolecules 1992, 25, 6277.
30. Wang, C. B.; Cooper, S. L. Macromolecules 1983, 16, 775.
31. Martin, D. J.; Meijs, G. F.; Renwick, G. M.; McCarthy, S. J.; Gunatillake, P. A. J Appl Polym Sci 1996, 62, 1377.
32. Miller, J. A.; Lin, S. B.; Hwang, K. K. S.; Wu, K. S.; Gibson, P. E.; Cooper, S. L. Macromolecules 1985, 18, 32.
33. Koberstein, J. T.; Galambos, A. F. Macromolecules 1992, 25, 5618.
34. Ng, H. N.; Allegrezza, A. E.; Seymour, R. W.; Cooper, S. L. Polymer 1973, 14, 255.
35. Eisenbach, C. D.; Baumgartner, M.; Gunter, C. In Advances in Elastomers and Rubber Elasticity; Lal, J.; Mark, J. E., Eds.; Plenum: New York, 1986; p 51.
36. Chen, T. K.; Shieh, T. S.; Chui, J. Y. Macromolecules 1998, 31, 1312.
37. Huh, D. S.; Cooper, S. L. Polym Eng Sci 1971, 11, 369.
38. Tien, Y. I.; Wei, K. H. J Appl Polym Sci 2002, 86, 1741.
39. Peebles, L. H. Macromolecules 1976, 9, 58.
40. Xie, W.; Hwu, J. M.; Jiang, G. J.; Buthelezi, T. M.; Pan, W. P. Polym Eng Sci 2003, 43, 214.
41. Artzi, N.; Nir, Y.; Narkis, M.; Siegmann, A. J Polym Sci Part B: Polym Phys 2002, 40, 1741.
42. Bershtein, V. A.; Egorova, L. M.; Yakushev, P. N.; Pissis, P.; Sysel, P.; Brozova, L. J Polym Sci Part B: Polym Phys 2002, 40, 1056.
43. Buxton, G. A.; Balazs, A. C. J Chem Phys 2002, 117, 7649.

44. Fornes, T. D.; Paul, D. R. Polymer 2003, 44, 4993.
45. Brandrup, J.; Immergut, E. H.; Grulke, E. A. Polymer Handbook; Wiley: New York, 1999.
46. Gunatillake, P. A.; Meijs, G. F.; McCarthy, S. J.; Adhikari, R. J Appl Polym Sci 2000, 76, 2026.
47. Briber, R. M.; Thomas, E. L. J Macromol Sci Phys 1983, 22, 509.
48. Xie, W.; Gao, Z. M.; Pan, W. P.; Hunter, D.; Singh, A.; Vaia, R. Chem Mater 2001, 13, 2979.
49. Ahagon, A. Rubber Chem Technol 1993, 66, 317.
50. Speckhard, T. A.; Cooper, S. L. Rubber Chem Technol 1986, 59, 405.
51. Lee, H. S.; Yoo, S. R.; Seo, S. W. J Polym Sci Part B: Polym Phys 1999, 37, 3233.
52. Paik Sung, C. S.; Smith, T. W.; Hu, C. B.; Sung, N. Macromolecules 1979, 12, 538.
53. Mullins, L. Rubber Chem Technol 1969, 42, 339.
54. Clement, F.; Bokobza, L.; Monnerie, L. Rubber Chem Technol 2001, 74, 847.
55. Bueche, F. J. J Appl Polym Sci 1960, 4, 107.
56. Dannenberg, E. M. Trans Inst Rubber Ind 1966, 42, 26.
57. Balazs, A. C.; Singh, C.; Zhulina, E. Macromolecules 1998, 31, 8370.
58. Vaia, R. A.; Giannelis, E. P. Macromolecules 1997, 30, 7990.
59. Vaia, R. A.; Giannelis, E. P. Macromolecules 1997, 30, 8000.